ACS APPLIED MATERIALS & INTERFACES

Research Article

www.acsami.org

Understanding the Halogenation Effects in Diketopyrrolopyrrole-Based Small Molecule Photovoltaics

Shi-Xin Sun,[†] Yong Huo,[†] Miao-Miao Li,[§] Xiaowen Hu,[‡] Hai-Jun Zhang,[§] You-Wen Zhang,[†] You-Dan Zhang,[†] Xiao-Long Chen,[†] Zi-Fa Shi,[†] Xiong Gong,*[,‡] Yongsheng Chen,[§] and Hao-Li Zhang*[,†]

[†]State Key Laboratory of Applied Organic Chemistry (SKLAOC), Key Laboratory of Special Function Materials and Structure Design (MOE), College of Chemistry and Chemical Engineering, Lanzhou University, Lanzhou, 730000, P. R. China

[‡]Department of Polymer Engineering, College of Polymer Science and Engneering and Department of Polymer Engineering, College of Polymer Science and Engineering, The University of Akron, Akron, Ohio 44236, United States

[§]Institute of Polymer Chemistry and Collaborative Innovation Center of Chemical Science and Engineering, College of Chemistry, Nankai University, Tianjin, 300071, P. R. China

Supporting Information

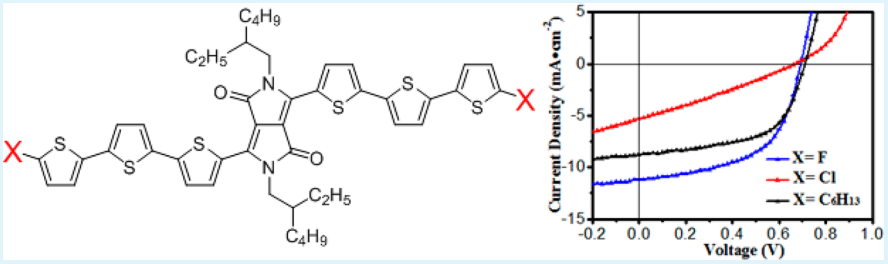

ABSTRACT: Two molecules containing a central diketopyrrolopyrrole and two oligothiophene units have been designed and synthesized. Comparisons between the molecules containing terminal F (FDPP) and Cl (CDPP) atoms allowed us to evaluate the effects of halogenation on the photovoltaic properties of the small molecule organic solar cells (OSCs). The OSCs devices employing FDPP:$PC_{71}BM$ films showed power conversion efficiencies up to 4.32%, suggesting that fluorination is an efficient method for constructing small molecules for OSCs.

KEYWORDS: *solution-processed small molecules, diketopyrrolopyrrole, organic solar cells, halogenation effect, device optimization*

INTRODUCTION

Organic solar cells (OSCs) offer great opportunities as renewable energy sources due to their attractive features, including low-cost large area fabrication, lightweight, and good mechanical flexibility.[1,2] Because of the fast development of new donor materials and interface layers as well as advances in device fabrication technologies, polymer-based OSCs have shown a dramatic increase of power conversion efficiencies (PCEs) reaching over 9% in single junctions[3−7] and 11% in tandem devices.[8] In parallel with polymer donor materials, solution-processable small molecules have been emerging as an attractive alternative to the widely studied polymeric counterparts,[9−21] which offer several unique advantages include well-defined molecular structures, definite molecular weight, higher purity, and good batch-to-batch reproducibility.[22,23]

Diketopyrrolopyrrole (DPP) chromophore is a widely used π-electron acceptor for OSC materials due to its favorable properties, e.g., strong light absorption, high photochemical stability, excellent charge carrier mobility.[20,24−27] Nguyen reported that a low band gap thiophene-based oligomer incorporating DPP chromophore, named SMDPPEH, achieved PCEs up to 3.0%,[28] which was the highest performance for the small molecule bulk heterojunction (BHJ) solar cells at that time. Much progresses have been made since then, and the highest PCEs of OSCs based-on DPP containing materials has reached 8.0% for polymer,[29] and 5.79% for small molecule.[25] It is highly desirable to improve the performance of DPP-based small molecule OSCs by modifying the oligomer architecture and optimizing the device fabrication.

Halogenation is a very widely adapted strategy for designing organic semiconductors.[30] Bao et al. have demonstrated that chlorination is a viable route to n-type materials owning to the inductive effect of chlorine and the presence of empty d-orbitals that allow the delocalization of the π-electron cloud.[31] Introducing F atom is also a widely used method in tailoring the properties of organic semiconductors[32,33] and polymer materials for OSCs.[34−36] Fluorination lowers the energy levels in conjugated systems, induces higher thermal stability, and has better electron transport performance.[36] In addition, it has also been reported that fluorine substituents reduce charge recombination and drive structure and morphology development.[34] However, in the research of small molecule OSCs, very

Received: April 22, 2015
Accepted: August 11, 2015
Published: August 11, 2015

DOI: 10.1021/acsami.5b03488
ACS Appl. Mater. Interfaces 2015, 7, 19914−19922

few halogenated molecules have been studied, so that the vital roles of halogenation in the molecular properties and device performance are not well understood.

To understand the halogenation effects on small molecule OSCs, we designed and synthesized two new thiophene-DPP-based low band gap small molecules. As shown in Figure 1, the

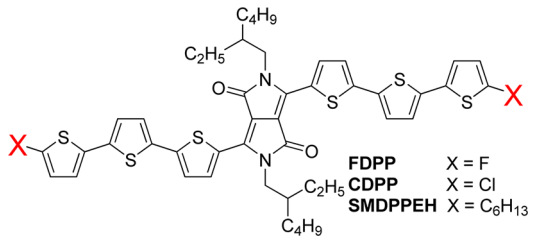

Figure 1. Chemical structures of FDPP, CDPP, and SMDPPEH.

new molecules have the identical conjugated framework as that of SMDPPEH,[28] while the terminal alkyl chains were replaced by F and Cl atoms, named as FDPP and CDPP, respectively. A systematic comparative investigation between the FDPP, CDPP, and SMDPPEH helps to unveil the effects of halogenation in the small molecule OSCs.

RESULTS AND DISCUSSION

Synthesis. The synthetic routes to the new molecules FDPP and CDPP are depicted in Scheme 1. The reference compound SMDPPEH was synthesized following a previously reported procedure.[37,38] The target molecule FDPP and CDPP were achieved through the Stille coupling reaction of DPP bromide with trimethyltin thiophene derivatives. The main challenge in the synthesis process was to synthesize and purify the asymmetric substituted intermediate compounds **5**, **6**, **9**, and **10**. The DPP dye **1** was used as a starting material and synthesized according to the literature procedure.[39] The compound **2** was obtained through the substitution reaction of 2-ethylhexyl bromide. Formation of the dibrominated DPP **3** was achieved by refluxing the chloroform solution of compound **2** and *N*-bromosuccinimide (NBS). We treated the compound **4** with *n*-butyl lithium (*n*-BuLi), followed by the addition of *N*-fluorobenzenesulfonimide (NFSI), which indeed afforded the monofluorinated **5** in 65% yield. However, besides compound **5**, the reaction also produced a considerable amount of difluorinated and unfluorinated compounds. The polarities of these three liquid compounds are very similar, and it is necessary to carefully separate the product **5** by column chromatography. The compound **5** was then subjected to bromination reaction with NBS and HOAc. The compound **9** was obtained handily from **8** by the Friedel–Crafts reaction. The reaction of **9** with NBS afforded compound **10**. The brominated compounds **6** and **10** were processed to the next reactions with *n*-BuLi through lithium-halogen exchange, followed by the substitution reaction with trimethyltin chloride to form the two important intermediates **7** and **11**, respectively. The Stille coupling reaction of the compounds **3** with **7** and **11** finally afforded the target molecule FDPP and CDPP in 80% and 63% yields, respectively.

Thermal Properties and Solubility. To assess the thermal stability and behavior of the target molecules, FDPP, CDPP, and SMDPPEH were characterized by the thermal gravimetric analysis (TGA) and differential scanning calorimetry (DSC). TGA analysis reveals that 5% weight-loss temperatures (T_d) of FDPP, CDPP, and SMDPPEH are 390, 378, and 384 °C, respectively (Figure 2a), indicating that all the three molecules are thermally stable enough for application in solar cells. The T_d has a sequence of FDPP > SMDPPEH > CDPP, suggesting that the fluorination enhanced thermal stability but chlorination does the opposite.

Thermal behaviors of the DPP-containing molecules have been further studied by DSC (Figure 2b). The main melting temperature (T_m) occurs at 198 °C (N_2 atmosphere) for FDPP and 159 °C for SMDPPEH. The CDPP shows an inconspicuous melting process at 184 °C (N_2 atmosphere). Upon the cooling process, FDPP and SMDPPEH exhibit a sharp crystallization exotherm at 158 and 134 °C, manifesting

Scheme 1. Synthesis Routes of FDPP and CDPP

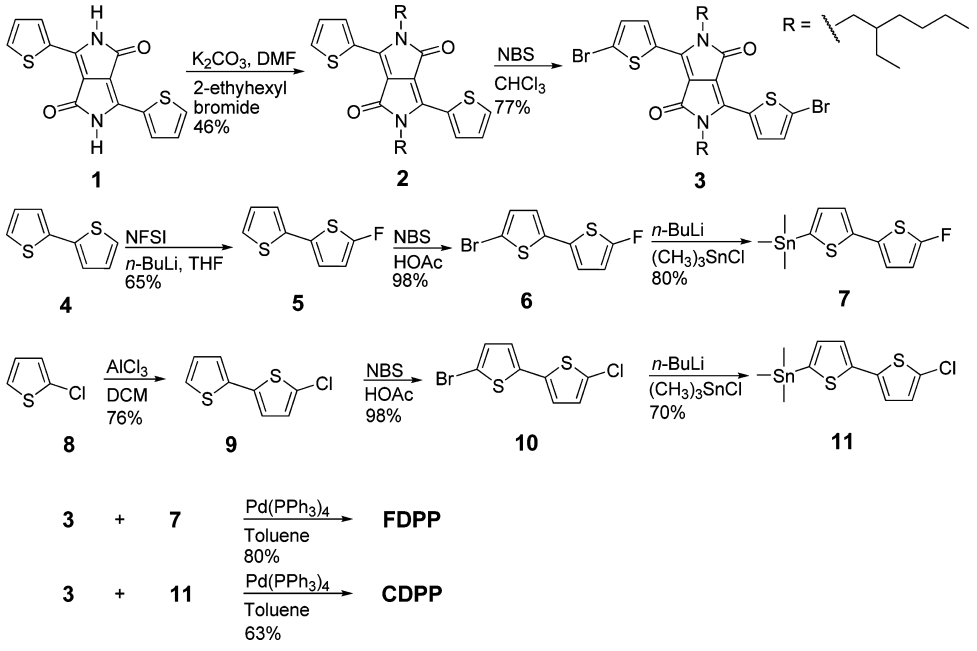

DOI: 10.1021/acsami.5b03488
ACS Appl. Mater. Interfaces 2015, 7, 19914–19922

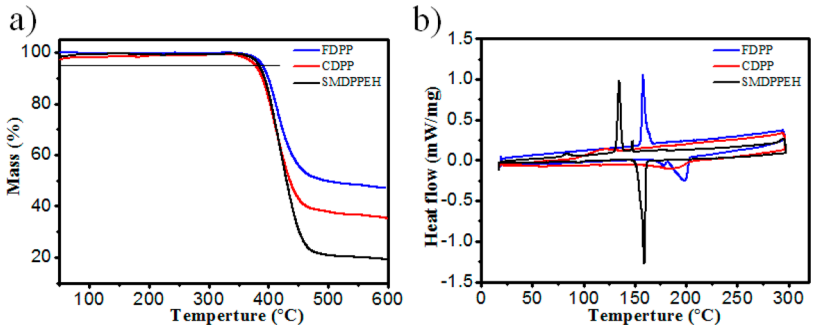

Figure 2. (a) TGA curves and (b) DSC thermograms for FDPP, CDPP, and SMDPPEH.

Table 1. Optical Absorption and Frontier Orbitals of Compounds FDPP, CDPP, and SMDPPEH

	thermal properties				optical absorption			frontier orbitals		
cmpd	T_d (°C)	T_m (°C)	T_c (°C)	solubility (mg/mL)	λ_{max} (f) (nm)	λ_{onset} (f) (nm)	bandgap (eV)	HOMO (eV)	LUMO (eV)	bandgap (eV)
FDPP	390	198	158	12	625	759	1.63	−5.17	−3.51	1.66
CDPP	378	184	123	6	620	752	1.65	−5.16	−3.49	1.67
SMDPPEH	384	159	134	>20	709	768	1.61	−5.12	−3.48	1.64

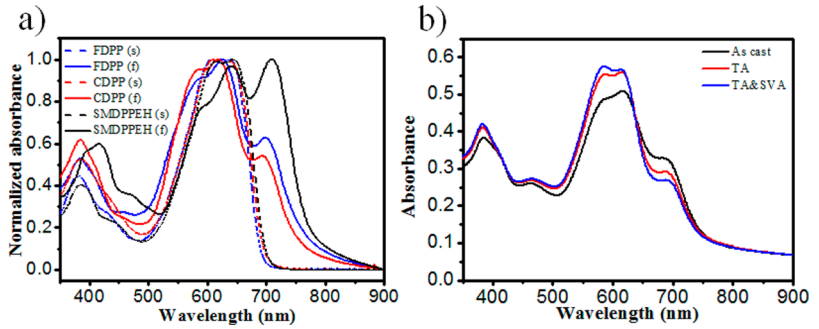

Figure 3. (a) UV−vis absorption spectra of FDPP, CDPP, and SMDPPEH in $CHCl_3$ solutions (s) and thin-films (f) and (b) UV−vis absorption spectra of FDPP:$PC_{71}BM$ blend films with different treatments.

that the two molecules have a strong tendency to crystallize. In contrast, CDPP shows an inconspicuous peak at 123 °C, which are typically correlated to the low crystallization ability. The distinction on thermal transitions is attributed to the differences in intermolecular interactions arising from the different end-substitutions. With the electronegative fluorine atom, the FDPP shows high thermal stability and intermolecular interactions via C−F···H and F···S interactions.[40]

The solubility of the compounds was determined in chloroform at room temperature by a reported method[41] and the results are listed in Table 1. As expected, the SMDPPEH shows the highest solubility owing to the flexible alkyl chains. Replacing the terminal alkyl chains with F and Cl significantly reduced the solubility. However, the FDPP shows a much higher solubility (12 mg/mL) than the CDPP (6 mg/mL), probably because the fluorine terminal atoms have a smaller surface energy.[42]

Optical Absorption and Frontier Orbital Levels. The solution and thin-films optical absorption spectra of the FDPP, CDPP, and SMDPPEH are presented in Figure 3a. In diluted chloroform solution, all of the DPP derivatives present two primary absorption bands in the range of approximately 300−450 nm and 500−700 nm, respectively. The absorption band at 500−700 nm is ascribed to the intramolecular charge transfer band between the DPP and thienyl moieties. The other absorption bands can be attributed to the $\pi-\pi^*$ transitions of the substituted thiophene moieties and their conjugation framwork.[43] The FDPP shows the maxima absorption (λ_{max}) at 608 nm in chloroform solution. After replacing the fluorine terminal with chlorine, the CDPP solution presents a very similar solution absorption profiles with the λ_{max} at 611 nm. The SMDPPEH exhibits a λ_{max} at 645 nm, slightly bathochromic shifted compared with other two compounds, which can be ascribed to the stronger electron donating ability of the alkyl substitution. Compared with the absorption character in solution, the absorption bands of the three compounds in thin-films are broadened with a strong bathochromic shift. Compound FDPP film exhibits absorption almost throughout the visible region with two peaks at 625 and 697 nm. A strong shoulder peak at around 697 nm indicates an effective $\pi-\pi$ packing between the molecule backbones at the solid state. The CDPP film also displays a broader absorption peak at 500−750 nm and the λ_{max} at 620 nm with a vibronic shoulder at 693 nm, suggesting that molecular self-organization behavior exist in the film. These two halogen terminal molecules display similar absorption profiles as well as the position of vibronic peaks. Compared with the above molecules, the absorption band of the SMDPPEH film exhibits obviously stronger intensity and bathochromic shift, showing the strongest absorption in the visible range with a λ_{max} at 709 nm.[28]

To test the absorption properties of the active layer, we have measured the absorption spectra of the FDPP and $PC_{71}BM$

DOI: 10.1021/acsami.5b03488
ACS Appl. Mater. Interfaces 2015, 7, 19914−19922

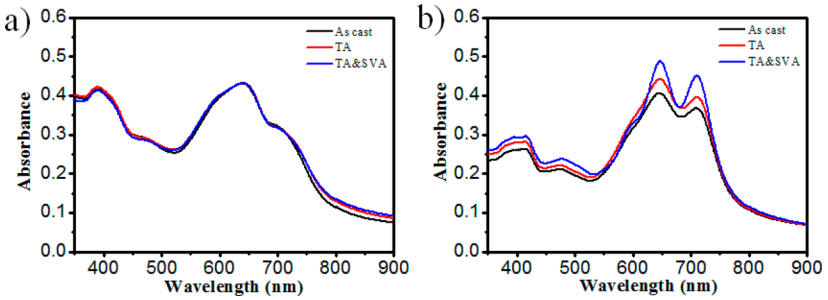

Figure 4. UV−vis absorption spectra of (a) CDPP:$PC_{71}BM$ and (b) SMDPPEH:$PC_{71}BM$ blend films with different treatments.

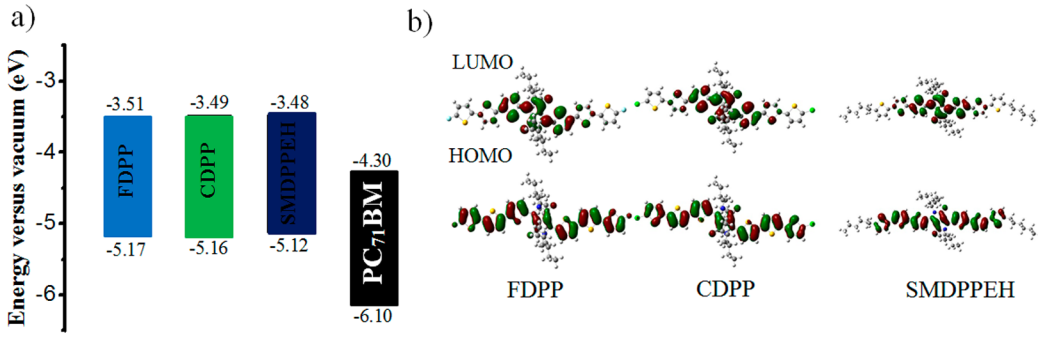

Figure 5. (a) Energy levels of FDPP, CDPP, SMDPPEH, and $PC_{71}BM$ and (b) electron density of HOMO and LUMO for FDPP, CDPP, and SMDPPEH computed by density functional theory (DFT).

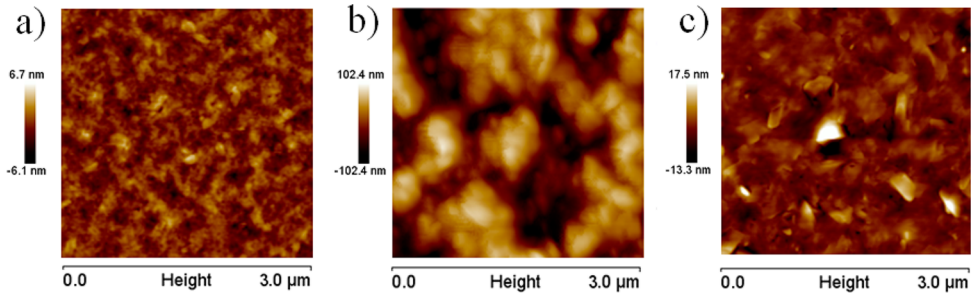

Figure 6. AFM images of TA&SVA annealed active layers: (a) FDPP, (b) CDPP, and (c) SMDPPEH. Scan size: 3 μm × 3 μm.

blend films upon various treatment methods (Figure 3b). The active layers were first deposited by spin-coating from chloroform solutions and then subjected to thermal annealing (TA) or thermal annealing followed by solvent vapor annealing (TA&SVA) methods. The absorption band at 690 nm for the as cast FDPP:$PC_{71}BM$ films steadily decreases and the strong absorption peaks around 586 and 614 nm increase with the TA treatment. With the TA&SVA treatment, the absorption profiles exhibits clear change and the 586 nm band become the λ_{max}, indicating that the aggregation of the as cast films eventually transforms into the thermodynamically more favored morphology.[44] However, the initial peak position and absorption intensity of the CDPP blend films do not have obvious change (Figure 4a) after the TA&SVA treatment. The SMDPPEH blend films show increased absorption peaks around 710 and 646 nm during the TA&SVA treatment of the active layers (Figure 4b).

Using the onset of optical absorption (λ_{onset}), optical bandgaps of the three DPP films are calculated ranging from 1.61 to 1.65 eV, as listed in Table 1. Frontier energy levels including the highest occupied molecular orbital (HOMO) and the lowest unoccupied molecular orbital (LUMO) measured (Figure 5) by cyclic voltammetry (Figure S3) are listed in Table 1. The energy levels of the HOMO and LUMO are −5.17 and −3.51 eV for FDPP, −5.16 and −3.49 eV for CDPP, −5.12 and −3.48 eV for SMDPPEH, respectively, as calculated from the onset oxidation potentials and onset reduction potentials. Frontier energy levels measured by cyclic voltammetry are in good agreement with the results from the UV−vis spectra. Introducing fluorine atom as the terminal group reduces both HOMO and LUMO energy levels compared with the SMDPPEH molecule.[45] Because of the strong inductive effect of F atoms, FDPP displays a lower LUMO energy level than CDPP. The electron density of the HOMO energy levels for FDPP distributes evenly over the entire conjugated framework, whereas that of the LUMO almost entirely localizes on the DPP unit.

Film Morphology. The morphology of the annealed blend films of the DPP-containing compounds was investigated by atomic force microscopy (AFM). As shown in Figure 6, the blend films exhibit surface roughness of 1.80 nm for FDPP, 32.8 nm for CDPP, and 2.49 nm for SMDPPEH. The relatively smoother surface is beneficial for exciton diffusion and dissociation in the blend films.[46] The CDPP films have a

DOI: 10.1021/acsami.5b03488
ACS Appl. Mater. Interfaces 2015, 7, 19914−19922

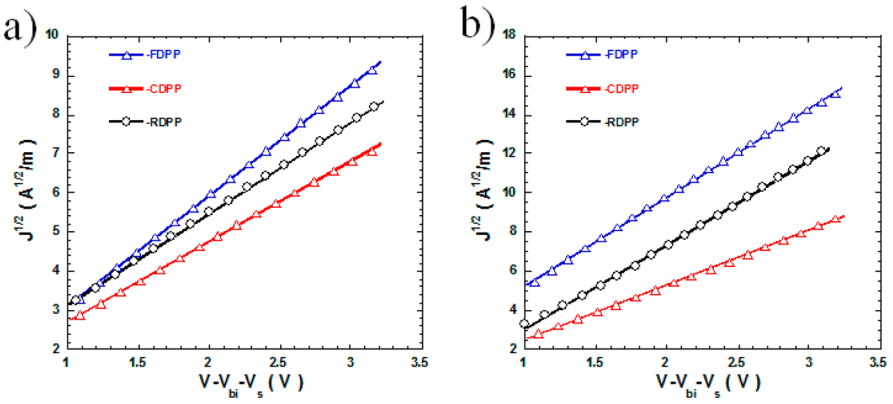

Figure 7. Current–voltage characteristics of (a) hole-only device and (b) electron-only devices for three DPP-containing compounds.

significantly higher roughness than the other two molecules due to its poor solubility.

Charge Carrier Mobility. To quantify carrier mobility for the DPP derivatives and $PC_{71}BM$ blend, current–voltage characteristics of single-carrier diodes were measured for blend materials in Figure 7. The hole and electron mobility were extracted using the space-charge limited current (SCLC) model summarized in Table 2.

Table 2. Hole and Electron Mobility of Three DPP-Containing Compounds

donor	μ_h ($cm^2\ V^{-1}\ S^{-1}$)	μ_e ($cm^2\ V^{-1}\ S^{-1}$)
FDPP	2.01×10^{-6}	5.37×10^{-6}
CDPP	0.96×10^{-6}	2.22×10^{-6}
SMDPPEH	1.60×10^{-6}	4.47×10^{-6}

For the FDPP:$PC_{71}BM$ blend, the hole and electron mobilities were found to be 2.01×10^{-6} $cm^2\ V^{-1}\ S^{-1}$ and 5.37×10^{-6} $cm^2\ V^{-1}\ S^{-1}$, respectively. Compared with FDPP:$PC_{71}BM$ blend, the hole and electron mobilities of CDPP: $PC_{71}BM$ blend were considerably smaller, whose hole mobility was only 0.96×10^{-6} $cm^2\ V^{-1}\ S^{-1}$. The device prepared from SMDPPEH:$PC_{71}BM$ blend exhibited hole and electron mobilities of 1.60×10^{-6} $cm^2\ V^{-1}\ S^{-1}$ and 4.47×10^{-6} $cm^2\ V^{-1}\ S^{-1}$, respectively. For both electron and hole mobilities, the three blend films had a sequence of FDPP:$PC_{71}BM$ > SMDPPEH:$PC_{71}BM$ > CDPP:$PC_{71}BM$. The much lower hole and electron mobilities of the CDPP:$PC_{71}BM$ blend film compared with that of FDPP:$PC_{71}BM$ and SMDPPEH:$PC_{71}BM$ can be attributed to the rough morphology and poor continuity of the films. The favorable high charge carrier mobility of the FDPP:$PC_{71}BM$ blend film is beneficial for charge transport, which is expected to lead to a high J_{sc}.[47]

Solar Cell Performance. To investigate the photovoltaic properties of the three small molecules, BHJ solar cells with a device structure of ITO/PEDOT:PSS/DPP:$PC_{71}BM$/PFN/Al were fabricated (PFN is poly [(9,9-bis(3′-(*N*,*N*-dimethylamino)propyl)-2,7-fluorene)-*alt*-2,7-(9,9-dioctylfluorene)][4]). The active layers of the devices were fabricated under a donor and acceptor weight ratio of 3:2, and the thermal annealing was conducted at 110 °C (Figures S5 and S6). The device characteristics with the active layer subjected to different treatments are summarized in Table 3, and the corresponding *J*–*V* curves of these devices are shown in Figure 8.

Table 3. Summary of Device Characteristics of FDPP, CDPP and SMDPPEH as Donor

cmpd	treatment	V_{oc} (V)	J_{sc} (mA cm^{-2})	FF (%)	PCE (%)
FDPP	as cast	0.79	8.41	43.8	2.92
FDPP	TA&SVA	0.69	11.17	55.6	4.32
CDPP	TA&SVA	0.67	5.29	28.4	1.00
SMDPPEH	TA&SVA	0.71	8.77	57.8	3.61

The SMDPPEH-based devices yielded a PCE of 3.61%, with an open circuit voltage (V_{oc}) of 0.71 V, a short circuit current (J_{sc}) of 8.77 mA cm^{-2}, and a fill factor (FF) of 57.8%. The PCE of our device is similar to that reported by Nguyen.[28] The as casted FDPP showed a moderate PCE of 2.92% with a V_{oc} of 0.79 V, a J_{sc} of 8.41 mA cm^{-2}, and a FF of 43.8%. After the TA&SVA treatment, the FDPP device exhibited a PCE of 4.32%, with a V_{oc} of 0.69 V, a J_{sc} of 11.17 mA cm^{-2} and a FF of 55.6%. The dramatically increased PCE is mainly attributed to the significant improvement of J_{sc} and FF. In contrast, after TA&SVA treatment, the CDPP:$PC_{71}BM$ blend films showed a PCE value of 1.00%, with a small V_{oc} of 0.67 V, a J_{sc} of 5.29 mA cm^{-2} and a FF of 28.4%. It can be seen that although the molecular structures and optical properties of FDPP and CDPP are very similar, difference in the halogenation substitution has a profound effect on their photovoltaic performance in BHJ solar cells. The devices based-on FDPP:$PC_{71}BM$ blend films with TA&SVA treatment give the highest PCEs among all the different devices, which stems from the ideal intermolecular interactions induce better film morphology. The low J_{sc}, FF, and PCEs of CDPP could be related to the inferior film quality owing to the low solubility.[43]

CONCLUSION

In conclusion, we have designed and synthesized two new solution-processable small molecules for BHJ OSCs. F or Cl substitution showed similar effects on the optical absorption and frontier orbital energy levels. However, the thermal properties, film morphology, and photovoltaic performance are significantly affected by the halogenation. The fluorinated molecule FDPP has a relatively high solubility and strong tendency to crystallize, which gives better film morphology, leading to the highest PCEs of 4.32%. However, the chlorinated molecule CDPP exhibits reduced thermal stability, lower solubility, which gives inferior film quality, resulting in poor device performance. This work demonstrates that introducing fluorine atoms onto the terminal segment of the small molecular backbone could be a promising method for efficient

DOI: 10.1021/acsami.5b03488
ACS Appl. Mater. Interfaces 2015, 7, 19914–19922

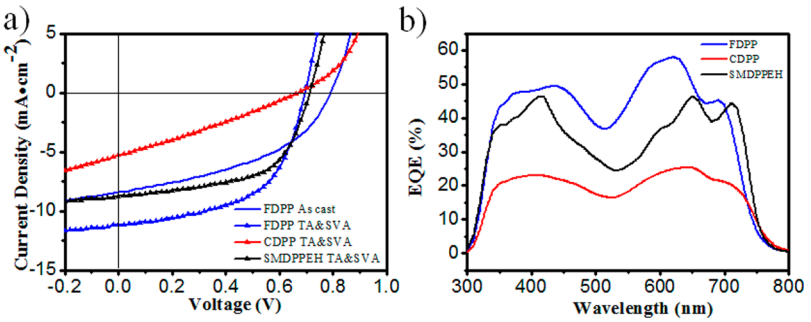

Figure 8. Current density voltage (J–V) curves and (b) external quantum efficiency (EQE) curves of FDPP, CDPP, and SMDPPEH as donor and $PC_{71}BM$ as acceptor subjected to TA&SVA treatment.

enhancement of the photovoltaic performance of BHJ small molecule OSCs.

EXPERIMENTAL SECTION

General Methods. Unless stated otherwise, all reactions and manipulations were carried out under argon atmosphere in flame-dried glassware. All starting materials, unless otherwise specified, were purchased from commercial suppliers and used without further purification. The solvents used were purified by distillation over the drying agents indicated and were transferred under argon atmosphere: THF ($MgSO_4$, Na), ethyl acetate, MeOH (Mg, I_2), DMF (CaH_2), toluene (Na), and deionized water. Flash chromatography: silica gel 60 (200–400 mesh).

Instrument. ^1H NMR and ^{13}C NMR were recorded on a Bruker 400 or 600 MHz spectrometer. The chemical shifts values (δ) were expressed in parts per million using residual solvent protons ($CDCl_3$: δ_H 7.26 ppm, δ_C 77.0 ppm). UV–vis absorption spectra were measured using a T6 UV–vis spectrometer. All cyclic voltammetry (CV) measurements were run on a CHI660C electrochemistry station (CHI) and carried out at room temperature with a conventional three-electrode, a platinum working electrode, a saturated $Ag/AgNO_3$ electrode as the reference electrode, and a Pt wire as counter electrode. Tetrabutylammonium phosphorus hexafluoride (Bu_4NPF_6, 0.1 M) in $CHCl_3$ solution was used as the supporting electrolyte, and the scan rate was 100 mV s^{-1}. Atomic force microscopy (AFM) was performed using Bruker MultiMode 8 in tapping mode. High-resolution mass spectral data (HRMS) were obtained on a Bruker APEX II FT–MS mass spectrometer. Thermo gravimetric analysis (TGA) measurements were performed on STA PT1600 from the Linseis company under a nitrogen flow at a heating rate of 10 °C min^{-1}. Differential scanning calorimetry (DSC) measurements were performed using a differential scanning calorimeter on DSC200F3 from the NETZSCH company under nitrogen at a heating rate of 5 °C min^{-1}. The organic molecule films on quartz used for absorption spectral measurement were prepared by spin-coating their chloroform solutions.

Device Fabrication. The photovoltaic devices was prepared by spin-casting the blend solution on ITO/PEDOT:PSS substrate. Approximately a 30 nm poly(3,4-ethylenedioxythiophene):poly-(styrenesulfonate) (PEDOT:PSS) layer was spin-coated onto the precleaned indium tin oxide (ITO) glass followed by thermal annealing at 150 °C for 10 min under ambient conditions. With active layers, DPP:$PC_{71}BM$ was made by spin coating chloroform solution with the molecular donor concentration of 5.5 mg/mL. The dried thin film was thermally annealed at 110 °C for 10 min with thermal annealing (TA) treatment. Followed the TA treatment, the blend films was exposed to chloroform vapor for 60 s with the TA&SVA treatment. A thin layer LiF (1 nm) or PFN and 100 nm Al layer were deposited on the DPP:$PC_{71}BM$ active layer under high vacuum (<2×10^{-4} Pa). The effective device area was measured to be 0.04 cm^2. The current density–voltage (J–V) characteristics were measured using a Keithley 2400 sourcemeter. Organic solar cells were characterized using a calibrated AM1.5G solar simulator (Oriel model 91192) with light intensity of 100 mW/cm^2. External quantum efficiencies (EQE) were measured using Stanford Research Systems SR810 lock-in amplifier.

The space charge limited current (SCLC) method was used to estimate the charge carrier mobility of FDPP, CDPP, and SMDPPEH thin films.[48] The structure of the hole-only diode is ITO/PEDOT:PSS/DPP:$PC_{71}BM$/MoO_3/Al, and the electron-only devices, ITO/Al/DPP:$PC_{71}BM$/Ca/Al, where Ag is silver and Al is aluminum, respectively. An approximately 100 nm thickness of DPP:$PC_{71}BM$ thin films was cast from an $CHCl_3$ solution. About 10 nm of MoO_3 and 100 nm of Al were sequentially deposited on top of the DPP:$PC_{71}BM$ layer in a vacuum system.

Synthesis. *2,5-Bis(2-ethylhexyl)-3,6-di(thiophen-2-yl)pyrrolo[3,4-c]pyrrole-1,4(2H,5H)-dione (**2**).* In an oven-dried two-necked 250 mL round-bottom flask, a mixture of 3,6-dithiophen-2-yl-2,5-dihy-dropyrrolo[3,4-*c*]pyrrole-1,4-dione (**1**, 7.61 g, 25.34 mmol) and anhydrous K_2CO_3 (11.41 g, 82.48 mmol) in anhydrous DMF (180 mL) was heated at 120 °C for 1 h. 2-Ethylhexyl bromide (13.52 g, 76.10 mmol) was then added dropwise. The reaction mixture was further stirred at 120 °C for 36 h, then cooled to room temperature and poured into distilled water (400 mL). After the resulting suspension stirred at room temperature for 1 h, the solid was collected by vacuum filtration, washed with several portions of distilled water and methanol, and then dried under vacuum. The crude product was purified by column chromatography (10:1 petroleum ether/ethyl acetate) to afford **2** as a dark red solid (6.10 g, 46%). The spectroscopic data match the previously reported in the literature.[39] ^1H NMR (400 MHz) δ: 8.89 (d, J = 3.6 Hz, 2H), 7.62 (d, J = 4.4 Hz, 2H), 7.27 (t, J = 4.4 Hz, 2H), 4.08–3.97 (m, 4H), 1.86–1.84 (m, 2H), 1.39–1.22 (m, 16H), 0.89–0.83 (m, 12H); MS (ESI) m/z (%): 525 ($[M + H]^+$).

*3,6-bis(5-Bromothiophen-2-yl)-2,5-bis(2-ethylhexyl)pyrrolo[3,4-c]pyrrole-1,4(2H,5H)-dione (**3**).* In a 500 mL double-neck round-bottom flask, compound **2** (7.56 g, 14.40 mmol) was dissolved in $CHCl_3$ (350 mL) and covered with aluminum foil. *N*-Bromosuccinimide (5.64 g, 31.68 mmol) was added in portions, and the reaction mixture was stirred overnight at 60 °C and then poured into water. The organic phase was separated and washed by water, dried ($MgSO_4$), and concentrated by rotary evaporation. The crude compound was purified by column chromatography (1:1 petroleum ether/dichloromethane) to afford **3** as a dark purple solid (7.56 g, 77%). The spectroscopic data match the previously reported data in the literature.[39] ^1H NMR (400 MHz) δ: 8.64 (d, J = 4.4 Hz, 2H), 7.21 (d, J = 4.0 Hz, 2H), 3.98–3.87 (m, 4H), 1.82–1.81 (m, 2H), 1.37–1.24 (m, 16H), 0.90–0.84 (m, 12H). MS (APCI) m/z (%): 681 (M^+).

*5-Fluoro-2,2′-bithiophene (**5**).* In an oven-dried two-necked 250 mL round-bottom flask, compound **4** (6.17 g, 37.15 mmol) in anhydrous THF (90 mL) was cooled to −78 °C, then *n*-BuLi (1.60 M hexane solution, 23.22 mL) was added dropwise at the same temperature. The mixture was stirred at 0 °C for 30 min and cooled again to −78 °C. After *N*-fluorobenzenesulfonimide (12.92 g, 40.97 mmol) was added, the reaction system was gradually warmed and stirred at room temperature for 24 h, then poured into ice-cold water. The mixture was extracted with hexane three times. The organic layers

DOI: 10.1021/acsami.5b03488
ACS Appl. Mater. Interfaces 2015, 7, 19914–19922

were washed with water and brine, dried ($MgSO_4$), then concentrated by rotary evaporation. The crude compound was purified by column chromatography (petroleum ether) to afford **5** as colorless oil (4.44 g, 65%). ^{1}H NMR (400 MHz) δ: 7.21 (d, J = 4.8 Hz, 1H), 7.08 (d, J = 3.2 Hz, 1H), 7.02−7.00 (m, 1H), 6.78 (t, J = 4 Hz, 1H), 6.42−6.43 (m, 1H). ^{13}C NMR (100 MHz) δ: 165.7, 162.8, 136.9, 127.7, 125.8, 124.3, 123.4, 119.8, 107.8. MS (EI) m/z (%): 184 (M^+, 100).

*5-Bromo-5′-fluoro-2,2′-bithiophene (**6**).* In a 250 mL double-neck round-bottom flask, compound **5** (5.52 g, 30 mmol) was dissolved in $CHCl_3$ (100 mL), then *N*-bromosuccinimide (6.41 g, 36 mmol) and HOAc (5 mL) were added. The reaction mixture was stirred at room temperature for 3 h and then poured into water, neutralized by saturation $NaHCO_3$ solution, and extracted with dichloromethane three times. The organic layer was washed with water and brine, dried ($MgSO_4$), then concentrated by rotary evaporation. The crude compound was purified by column chromatography (petroleum ether) to afford **6** as a white solid (7.65 g, 98%). Mp 59−60 °C. ^{1}H NMR (400 MHz) δ: 6.95 (d, J = 4 Hz, 1H), 6.79 (d, J = 4 Hz, 1H), 6.69 (t, J = 4 Hz, 1H), 6.41−6.39 (m, 1H). ^{13}C NMR (100 MHz) δ: 166.0, 163.1, 138.4, 130.5, 124.9, 123.5, 120.3, 110.9, 108.0, 107.9. HRMS (c ESI) m/z calcd for $C_8H_4BrFS_2$ $[M]^+$ 261.8916; found, 261.8919.

*(5′-Fluoro-2,2′-bithiophen-5-yl)trimethylstannane (**7**).* In an oven-dried two-necked 50 mL round-bottom flask, compound **6** (263 mg, 1 mmol) and *N*,*N*,*N*′,*N*′-tetramethylethylenediamine (TMEDA) (0.23 mL, 1.5 mmol) in anhydrous THF (10 mL) was cooled to 0 °C. *n*-BuLi (2.40 M hexane solution, 0.65 mL) was added dropwise and the mixture was stirred at 0 °C for 2 h. Me_3SnCl (1.0 M in hexane, 1.2 mL, 1.2 mmol) was then added and the solution stirred overnight. The reaction mixture was then filtered and rinsed with hexane to afford compound **7** as the yellow solid (277 mg, 80%). Mp 76−78 °C. ^{1}H NMR (400 MHz) δ: 7.16 (d, J = 3.2 Hz, 1H), 7.07 (d, J = 3.2 Hz, 1H), 6.75 (t, J = 4 Hz, 1H), 6.41−6.39 (m, 1H), 0.39 (s, 9H). ^{13}C NMR (100 MHz) δ: 165.6, 162.8, 142.5, 137.5, 135.7, 126.1, 124.6, 119.5, 107.8, 107.7, −8.24. HRMS (c ESI) m/z calcd for $C_{11}H_{13}FS_2Sn$ $[M]^+$ 347.9459; found, 347.9463.

*5-Chloro-2,2′-bithiophene (**9**).* To a 140 mL dry dichloromethane solution of **8** (9.96 g, 84 mmol) were added $AlCl_3$ (11.20 g, 84 mmol) at room temperature. After the mixture was stirred at reflux for 2 h, the solvent was removed under vacuum. The crude compound was purified by column chromatography (petroleum ether) to afford **9** as a colorless oil at room temperature (12.76 g, 76%). ^{1}H NMR (400 MHz) δ: 7.04 (d, J = 4.8 Hz, 1H), 6.93 (d, J = 3.6 Hz, 1H), 6.85−6.82 (m, 1H), 6.76 (d, J = 4 Hz, 1H), 6.66 (d, J = 4 Hz, 1H). ^{13}C NMR (100 MHz) δ: 136.3, 135.9, 128.4, 127.6, 126.7, 124.5, 123.7, 122.6. MS (EI) m/z (%): 200 (M^+, 100).

*5-Bromo-5′-chloro-2,2′-bithiophene (**10**).* In a 250 mL double-neck round-bottom flask, compound **5** (6.01 g, 30 mmol) was dissolved in $CHCl_3$ (100 mL), then *N*-bromosuccinimide (6.41 g, 36 mmol) and HOAc (5 mL) were added. The reaction mixture was stirred at room temperature for 3 h, then poured into water, neutralized by a saturated $NaHCO_3$ solution, and extracted with dichloromethane three times. The organic layer was washed with water and brine, dried ($MgSO_4$), then concentrated by rotary evaporation. The crude compound was purified by column chromatography (petroleum ether) to afford **10** as a white solid (8.13 g, 98%). ^{1}H NMR (400 MHz) δ: 6.96 (d, J = 3.6 Hz, 1H), 6.86 (d, J = 4 Hz, 1H), 6.84−6.81 (m, 2H). ^{13}C NMR (100 MHz) δ: 137.9, 134.9, 130.6, 129.3, 126.9, 124.0, 123.2, 111.4. MS (EI) m/z (%): 280 (M^+, 100).

*(5′-Chloro-2,2′-bithiophen-5-yl)trimethylstannane (**11**).* In an oven-dried two-necked 50 mL round-bottom flask, compound **10** (279 mg, 1 mmol) and TMEDA (0.23 mL, 1.5 mmol) in anhydrous THF (10 mL) was cooled to 0 °C. *n*-BuLi (2.40 M hexane solution, 0.65 mL) was added dropwise and the mixture was stirred at 0 °C for 2 h. Me_3SnCl (1.0 M in hexane, 1.2 mL, 1.2 mmol) was then added and the solution stirred overnight. The reaction mixture was then filtered and rinsed with hexane to afford compound **11** as the yellow solid (254 mg, 70%). Mp 70−72 °C. ^{1}H NMR (400 MHz) δ: 7.22−7.19 (m, 1H), 7.08 (d, J = 3.2 Hz, 1H), 6.92 (d, J = 4 Hz, 1H), 6.82 (d, J = 4 Hz, 1H), 0.39 (s, 9H). ^{13}C NMR (100 MHz) δ: 141.9, 138.0, 136.2, 135.8, 128.3, 126.8, 125.1, 122.6, −8.23. HRMS (c ESI) m/z calcd for $C_{11}H_{13}ClS_2Sn$ $[M]^+$ 363.9164; found, 363.9171.

FDPP. In an oven-dried two-necked 50 mL round-bottom flask, compounds **3** (341 mg, 0.50 mmol) and **7** (382 mg, 1.10 mmol) and $Pd(PPh_3)_4$ (57 mg, 0.05 mmol) were added to toluene (30 mL) which was degassed for 30 min. The reaction mixture was stirred at 110 °C for 12 h and then cooled to room temperature. The solvent was removed under vacuum. The crude compound was purified by column chromatography (3:1 petroleum ether/dichloromethane) to afford **FDPP** as a dark-blue powder (355 mg, 80%); ^{1}H NMR (400 MHz) δ: 9.11−8.70 (s, 2H), 7.25−7.13 (m, 4H), 6.98 (s, 2H), 6.85−6.77 (m, 2H), 6.44 (m, 2H), 4.15−3.95 (m, 4H), 1.93−1.90 (m, 2H), 1.39−1.28 (m, 16H), 0.94−0.86 (m, 12H). ^{13}C NMR (150 MHz) δ: 165.7, 163.9, 161.8, 141.5, 140.5, 139.3, 137.8, 136.7, 134.8, 134.6, 128.2, 125.7, 125.3, 124.7, 124.2, 120.5, 108.2, 45.9, 39.3, 30.4, 28.6, 23.6, 23.1, 14.1, 10.6. HRMS (c ESI) m/z calcd for $C_{46}H_{46}F_2N_2O_2S_6$ $[M + H]^+$ 889.1924; found, 889.1917. Elemental analysis calcd for $C_{46}H_{46}F_2N_2O_2S_6$, C, 62.13, H, 5.21, N, 3.15; found, C, 61.95, H, 4.98, N, 2.90.

CDPP. In an oven-dried two-necked 50 mL round-bottom flask, compounds **3** (341 mg, 0.50 mmol) and **11** (399 mg, 1.10 mmol) and $Pd(PPh_3)_4$ (57 mg, 0.05 mmol) were added to toluene (30 mL) which was degassed for 30 min. The reaction mixture was further stirred at 110 °C for 12 h and then cooled to room temperature. The solvent was removed under vacuum. The crude compound was purified by column chromatography (3:1 petroleum ether/dichloromethane) to afford **CDPP** as a dark-blue powder (290 mg, 63%). ^{1}H NMR (600 MHz) δ: 8.92 (d, J = 4.2 Hz, 2H), 7.27 (d, J = 5.4 Hz, 2H), 7.19 (d, J = 3.6 Hz, 2H), 7.03 (d, J = 3.6 Hz, 2H), 6.96 (d, J = 3.6 Hz, 2H), 6.85 (d, J = 3.6 Hz, 2H), 4.08−3.98 (m, 4H), 1.92−1.89 (m, 2H), 1.40−1.28 (m, 16H), 0.94−0.86 (m, 12H). The compound shows high opacity and poor solubility to record a carbon NMR spectrum. HRMS (c ESI) m/z calcd for $C_{46}H_{46}Cl_2N_2O_2S_6$ $[M]^+$ 920.1255; found, 920.1246. Elemental analysis calcd for $C_{46}H_{46}Cl_2N_2O_2S_6$, C, 59.91, H, 5.03, N, 3.04; found, C, 59.59, H, 4.76, N, 2.75.

■ ASSOCIATED CONTENT

Supporting Information

The Supporting Information is available free of charge on the ACS Publications website at DOI: 10.1021/acsami.5b03488.

Details of ^{1}H and ^{13}C NMR spectra, UV−vis absorption spectra, and additional J−V characteristics (PDF)

■ AUTHOR INFORMATION

Corresponding Authors

*E-mail: haoli.zhang@lzu.edu.cn.

*E-mail: xgong@uakron.edu.

Author Contributions

The manuscript was written through contributions of all authors. All authors have given approval to the final version of the manuscript.

Notes

The authors declare no competing financial interest.

■ ACKNOWLEDGMENTS

This work is supported by National Basic Research Program of China (973 Program) Grant No. 2012CB933102, National Natural Science Foundation of China (NSFC Grants 21233001 and 21190034), and the Fundamental Research Funds for the Central Universities and 111 Project.

■ REFERENCES

(1) Dam, H. F.; Andersen, T. R.; Pedersen, E. B. L.; Thydén, K. T. S.; Helgesen, M.; Carlé, J. E.; Jørgensen, P. S.; Reinhardt, J.; Søndergaard, R. R.; Jørgensen, M.; Bundgaard, E.; Krebs, F. C.; Andreasen, J. W.

DOI: 10.1021/acsami.5b03488
ACS Appl. Mater. Interfaces 2015, 7, 19914−19922

Enabling Flexible Polymer Tandem Solar Cells by 3D Ptychographic Imaging. *Adv. Eng. Mater.* **2015**, *5*, 1400736.
(2) Wu, J.-S.; Cheng, S.-W.; Cheng, Y.-J.; Hsu, C.-S. Donor-acceptor conjugated polymers based on multifused ladder-type arenes for organic solar cells. *Chem. Soc. Rev.* **2015**, *44*, 1113−1154.
(3) Liu, Y.; Zhao, J.; Li, Z.; Mu, C.; Ma, W.; Hu, H.; Jiang, K.; Lin, H.; Ade, H.; Yan, H. Aggregation and morphology control enables multiple cases of high-efficiency polymer solar cells. *Nat. Commun.* **2014**, *5*, 5293−5260.
(4) He, Z.; Zhong, C.; Su, S.; Xu, M.; Wu, H.; Cao, Y. Enhanced power-conversion efficiency in polymer solar cells using an inverted device structure. *Nat. Photon.* **2012**, *6*, 591−595.
(5) Li, K.; Li, Z.; Feng, K.; Xu, X.; Wang, L.; Peng, Q. Development of Large Band-Gap Conjugated Copolymers for Efficient Regular Single and Tandem Organic Solar Cells. *J. Am. Chem. Soc.* **2013**, *135*, 13549−13557.
(6) Nguyen, T. L.; Choi, H.; Ko, S. J.; Uddin, M. A.; Walker, B.; Yum, S.; Jeong, J. E.; Yun, M. H.; Shin, T. J.; Hwang, S.; Kim, J. Y.; Woo, H. Y. Semi-crystalline photovoltaic polymers with efficiency exceeding 9% in a 300 nm thick conventional single-cell device. *Energy Environ. Sci.* **2014**, *7*, 3040−3051.
(7) You, J.; Dou, L.; Yoshimura, K.; Kato, T.; Ohya, K.; Moriarty, T.; Emery, K.; Chen, C.-C.; Gao, J.; Li, G.; Yang, Y. A polymer tandem solar cell with 10.6% power conversion efficiency. *Nat. Commun.* **2013**, *4*, 1446−1455.
(8) Chen, C. C.; Chang, W. H.; Yoshimura, K.; Ohya, K.; You, J.; Gao, J.; Hong, Z.; Yang, Y. An efficient triple-junction polymer solar cell having a power conversion efficiency exceeding 11%. *Adv. Mater.* **2014**, *26*, 5670−5677.
(9) Yu, Q.-C.; Fu, W.-F.; Wan, J.-H.; Wu, X.-F.; Shi, M.-M.; Chen, H.-Z. Evaluation of Heterocycle-Modified Pentathiophene-Based Molecular Donor Materials for Solar Cells. *ACS Appl. Mater. Interfaces* **2014**, *6*, 5798−5809.
(10) Sun, Y.; Welch, G. C.; Leong, W. L.; Takacs, C. J.; Bazan, G. C.; Heeger, A. J. Solution-processed small-molecule solar cells with 6.7% efficiency. *Nat. Mater.* **2012**, *11*, 44−48.
(11) Zhang, Y.; Deng, D.; Lu, K.; Zhang, J.; Xia, B.; Zhao, Y.; Fang, J.; Wei, Z. Synergistic Effect of Polymer and Small Molecules for High-Performance Ternary Organic Solar Cells. *Adv. Mater.* **2015**, *27*, 1071−1076.
(12) Mercier, L. G.; Mishra, A.; Ishigaki, Y.; Henne, F.; Schulz, G.; Bäuerle, P. Acceptor-Donor-Acceptor Oligomers Containing Dithieno-[3,2-b:2′,3′-d]pyrrole and Thieno[2,3-c]pyrrole-4,6-dione Units for Solution-Processed Organic Solar Cells. *Org. Lett.* **2014**, *16*, 2642−2645.
(13) Zhang, Q.; Kan, B.; Liu, F.; Long, G.; Wan, X.; Chen, X.; Zuo, Y.; Ni, W.; Zhang, H.; Li, M.; Hu, Z.; Huang, F.; Cao, Y.; Liang, Z.; Zhang, M.; Russell, T. P.; Chen, Y. Small-molecule solar cells with efficiency over 9%. *Nat. Photon.* **2015**, *9*, 35−41.
(14) Shen, S.; Jiang, P.; He, C.; Zhang, J.; Shen, P.; Zhang, Y.; Yi, Y.; Zhang, Z.; Li, Z.; Li, Y. Solution-Processable Organic Molecule Photovoltaic Materials with Bithienyl-benzodithiophene Central Unit and Indenedione End Groups. *Chem. Mater.* **2013**, *25*, 2274−2281.
(15) Mei, J.; Graham, K. R.; Stalder, R.; Reynolds, J. R. Synthesis of Isoindigo-Based Oligothiophenes for Molecular Bulk Heterojunction Solar Cells. *Org. Lett.* **2010**, *12*, 660−663.
(16) Sun, K.; Xiao, Z.; Lu, S.; Zajaczkowski, W.; Pisula, W.; Hanssen, E.; White, J. M.; Williamson, R. M.; Subbiah, J.; Ouyang, J.; Holmes, A. B.; Wong, W. W. H.; Jones, D. J. A molecular nematic liquid crystalline material for high-performance organic photovoltaics. *Nat. Commun.* **2015**, *6*, 6013.
(17) Lin, L. Y.; Chen, Y. H.; Huang, Z. Y.; Lin, H. W.; Chou, S. H.; Lin, F.; Chen, C. W.; Liu, Y. H.; Wong, K. T. A low-energy-gap organic dye for high-performance small-molecule organic solar cells. *J. Am. Chem. Soc.* **2011**, *133*, 15822−15825.
(18) Lim, N.; Cho, N.; Paek, S.; Kim, C.; Lee, J. K.; Ko, J. High-Performance Organic Solar Cells with Efficient Semiconducting Small Molecules Containing an Electron-Rich Benzodithiophene Derivative. *Chem. Mater.* **2014**, *26*, 2283−2288.
(19) Qin, H.; Li, L.; Guo, F.; Su, S.; Peng, J.; Cao, Y.; Peng, X. Solution-processed bulk heterojunction solar cells based on a porphyrin small molecule with 7% power conversion efficiency. *Energy Environ. Sci.* **2014**, *7*, 1397−1401.
(20) Du, Z.; Chen, W.; Wen, S.; Qiao, S.; Liu, Q.; Ouyang, D.; Wang, N.; Bao, X.; Yang, R. New Benzo[1,2-b:4,5-b′]dithiophene-Based Small Molecules Containing Alkoxyphenyl Side Chains for High Efficiency Solution-Processed Organic Solar Cells. *ChemSusChem* **2014**, *7*, 3319−3327.
(21) Patra, D.; Huang, T.-Y.; Chiang, C.-C.; Maturana, R. O. V.; Pao, C.-W.; Ho, K.-C.; Wei, K.-H.; Chu, C.-W. 2-Alkyl-5-thienyl-Substituted Benzo[1,2-b:4,5-b′]dithiophene-Based Donor Molecules for Solution-Processed Organic Solar Cells. *ACS Appl. Mater. Interfaces* **2013**, *5*, 9494−9500.
(22) Lin, Y.; Li, Y.; Zhan, X. Small molecule semiconductors for high-efficiency organic photovoltaics. *Chem. Soc. Rev.* **2012**, *41*, 4245−4272.
(23) Roncali, J.; Leriche, P.; Blanchard, P. Molecular Materials for Organic Photovoltaics: Small is Beautiful. *Adv. Mater.* **2014**, *26*, 3821−3838.
(24) Huang, J.; Zhan, C.; Zhang, X.; Zhao, Y.; Lu, Z.; Jia, H.; Jiang, B.; Ye, J.; Zhang, S.; Tang, A.; Liu, Y.; Pei, Q.; Yao, J. Solution-Processed DPP-Based Small Molecule that Gives High Photovoltaic Efficiency with Judicious Device Optimization. *ACS Appl. Mater. Interfaces* **2013**, *5*, 2033−2039.
(25) Lin, Y.; Ma, L.; Li, Y.; Liu, Y.; Zhu, D.; Zhan, X. A Solution-Processable Small Molecule Based on Benzodithiophene and Diketopyrrolopyrrole for High-Performance Organic Solar Cells. *Adv. Eng. Mater.* **2013**, *3*, 1166−1170.
(26) Hendriks, K. H.; Li, W.; Wienk, M. M.; Janssen, R. A. J. Small-Bandgap Semiconducting Polymers with High Near-Infrared Photoresponse. *J. Am. Chem. Soc.* **2014**, *136*, 12130−12136.
(27) Lee, O. P.; Yiu, A. T.; Beaujuge, P. M.; Woo, C. H.; Holcombe, T. W.; Millstone, J. E.; Douglas, J. D.; Chen, M. S.; Frechet, J. M. Efficient small molecule bulk heterojunction solar cells with high fill factors via pyrene-directed molecular self-assembly. *Adv. Mater.* **2011**, *23*, 5359−5363.
(28) Tamayo, A. B.; Dang, X.-D.; Walker, B.; Seo, J.; Kent, T.; Nguyen, T.-Q. A low band gap, solution processable oligothiophene with a dialkylated diketopyrrolopyrrole chromophore for use in bulk heterojunction solar cells. *Appl. Phys. Lett.* **2009**, *94*, 103301.
(29) Hendriks, K. H.; Heintges, G. H. L.; Gevaerts, V. S.; Wienk, M. M.; Janssen, R. A. J. High-Molecular-Weight Regular Alternating Diketopyrrolopyrrole-based Terpolymers for Efficient Organic Solar Cells. *Angew. Chem., Int. Ed.* **2013**, *52*, 8341−8344.
(30) Liu, Y.-Y.; Song, C.-L.; Zeng, W.-J.; Zhou, K.-G.; Shi, Z.-F.; Ma, C.-B.; Yang, F.; Zhang, H.-L.; Gong, X. High and Balanced Hole and Electron Mobilities from Ambipolar Thin-Film Transistors Based on Nitrogen-Containing Oligoacences. *J. Am. Chem. Soc.* **2010**, *132*, 16349−16351.
(31) Tang, M. L.; Bao, Z. Halogenated Materials as Organic Semiconductors. *Chem. Mater.* **2011**, *23*, 446−455.
(32) van der Poll, T. S.; Love, J. A.; Nguyen, T.-Q.; Bazan, G. C. Non-Basic High-Performance Molecules for Solution-Processed Organic Solar Cells. *Adv. Mater.* **2012**, *24*, 3646−3649.
(33) Liu, X.; Hsu, B. B. Y.; Sun, Y.; Mai, C.-K.; Heeger, A. J.; Bazan, G. C. High Thermal Stability Solution-Processable Narrow-Band Gap Molecular Semiconductors. *J. Am. Chem. Soc.* **2014**, *136*, 16144−16147.
(34) Stuart, A. C.; Tumbleston, J. R.; Zhou, H.; Li, W.; Liu, S.; Ade, H.; You, W. Fluorine Substituents Reduce Charge Recombination and Drive Structure and Morphology Development in Polymer Solar Cells. *J. Am. Chem. Soc.* **2013**, *135*, 1806−1815.
(35) Guo, S.; Ning, J.; Körstgens, V.; Yao, Y.; Herzig, E. M.; Roth, S. V.; Müller-Buschbaum, P. The Effect of Fluorination in Manipulating the Nanomorphology in PTB7:PC71BM Bulk Heterojunction Systems. *Adv. Eng. Mater.* **2015**, DOI: 10.1002/aenm.201401315.
(36) Zhou, H.; Yang, L.; You, W. Rational Design of High Performance Conjugated Polymers for Organic Solar Cells. *Macromolecules* **2012**, *45*, 607−632.

DOI: 10.1021/acsami.5b03488
ACS Appl. Mater. Interfaces 2015, 7, 19914−19922

(37) Tantiwiwat, M.; Tamayo, A.; Luu, N.; Dang, X.-D.; Nguyen, T.-Q. Oligothiophene Derivatives Functionalized with a Diketopyrrolopyrrolo Core for Solution-Processed Field Effect Transistors: Effect of Alkyl Substituents and Thermal Annealing. *J. Phys. Chem. C* **2008**, *112*, 17402−17407.
(38) Zerdan, R. B.; Shewmon, N. T.; Zhu, Y.; Mudrick, J. P.; Chesney, K. J.; Xue, J.; Castellano, R. K. The Influence of Solubilizing Chain Stereochemistry on Small Molecule Photovoltaics. *Adv. Funct. Mater.* **2014**, *24*, 5993−6004.
(39) Huo, L.; Hou, J.; Chen, H.-Y.; Zhang, S.; Jiang, Y.; Chen, T. L.; Yang, Y. Bandgap and Molecular Level Control of the Low-Bandgap Polymers Based on 3,6-Dithiophen-2-yl-2,5-dihydropyrrolo[3,4-c]-pyrrole-1,4-dione toward Highly Efficient Polymer Solar Cells. *Macromolecules* **2009**, *42*, 6564−6571.
(40) Reichenbacher, K.; Suss, H. I.; Hulliger, J. Fluorine in crystal engineering-"the little atom that could". *Chem. Soc. Rev.* **2005**, *34*, 22−30.
(41) Walker, B.; Tamayo, A.; Duong, D. T.; Dang, X.-D.; Kim, C.; Granstrom, J.; Nguyen, T.-Q. A Systematic Approach to Solvent Selection Based on Cohesive Energy Densities in a Molecular Bulk Heterojunction System. *Adv. Eng. Mater.* **2011**, *1*, 221−229.
(42) Duan, C.; Huang, F.; Cao, Y. Recent development of push−pull conjugated polymers for bulk-heterojunction photovoltaics: rational design and fine tailoring of molecular structures. *J. Mater. Chem.* **2012**, *22*, 10416−10434.
(43) Liu, J.; Walker, B.; Tamayo, A.; Zhang, Y.; Nguyen, T.-Q. Effects of Heteroatom Substitutions on the Crystal Structure, Film Formation, and Optoelectronic Properties of Diketopyrrolopyrrole-Based Materials. *Adv. Funct. Mater.* **2013**, *23*, 47−56.
(44) Shin, W.; Yasuda, T.; Watanabe, G.; Yang, Y. S.; Adachi, C. Self-Organizing Mesomorphic Diketopyrrolopyrrole Derivatives for Efficient Solution-Processed Organic Solar Cells. *Chem. Mater.* **2013**, *25*, 2549−2556.
(45) Albrecht, S.; Janietz, S.; Schindler, W.; Frisch, J.; Kurpiers, J.; Kniepert, J.; Inal, S.; Pingel, P.; Fostiropoulos, K.; Koch, N.; Neher, D. Fluorinated Copolymer PCPDTBT with Enhanced Open-Circuit Voltage and Reduced Recombination for Highly Efficient Polymer Solar Cells. *J. Am. Chem. Soc.* **2012**, *134*, 14932−14944.
(46) Kan, B.; Li, M.; Zhang, Q.; Liu, F.; Wan, X.; Wang, Y.; Ni, W.; Long, G.; Yang, X.; Feng, H.; Zuo, Y.; Zhang, M.; Huang, F.; Cao, Y.; Russell, T. P.; Chen, Y. A Series of Simple Oligomer-like Small Molecules Based on Oligothiophenes for Solution-Processed Solar Cells with High Efficiency. *J. Am. Chem. Soc.* **2015**, *137*, 3886−3893.
(47) Guo, X.; Zhou, N.; Lou, S. J.; Smith, J.; Tice, D. B.; Hennek, J. W.; Ortiz, R. P.; Navarrete, J. T. L.; Li, S.; Strzalka, J.; Chen, L. X.; Chang, R. P. H.; Facchetti, A.; Marks, T. J. Polymer solar cells with enhanced fill factors. *Nat. Photonics* **2013**, *7*, 825−833.
(48) Liu, C.; Yi, C.; Wang, K.; Yang, Y.; Bhatta, R. S.; Tsige, M.; Xiao, S.; Gong, X. Single-Junction Polymer Solar Cells with Over 10% Efficiency by a Novel Two-Dimensional Donor−Acceptor Conjugated Copolymer. *ACS Appl. Mater. Interfaces* **2015**, *7*, 4928−4935.

DOI: 10.1021/acsami.5b03488
ACS Appl. Mater. Interfaces 2015, 7, 19914−19922